Chapter 3

Dilute Fe doped $Ge_{1-x}Sb_x$ alloy thin film system

The present chapter discusses, the study of dilute Iron doped Germanium rich GeSb alloy thin films i. e. $Fe_{0.01}Ge_{1-x}Sb_x$, grown on Silicon substrate using physical vapor deposition technique. This chapter is divided in two parts.

Part I, Dilute Fe doped $Ge_{1-x}Sb_x$ alloy thin films: *In this section the effects of Antimony concentration variations in $Fe_{0.01}Ge_{1-x}Sb_x$ thin films grown on Si substrate using thermal evaporation technique have been discussed. Various characterization studies of the $Fe_{0.01}Ge_{1-x}Sb_x$ thin films such as structural, electrical, surface morphology and magnetic studies are discussed in detail.*

Part II, Irradiation effects of SHI beam on $Fe_{0.01}Ge_{1-x}Sb_x$ alloy thin films: *This section describes the comparatively study of un-irradiated and irradiated dilute Iron doped $Ge_{1-x}Sb_x$ ($x = 0.01$ and 0.10) semiconducting alloy thin films. A Comparative study of un-irradiated and irradiated films on structural, electrical and surface morphology properties of the films is done using various techniques.*

3.1 $Fe_{0.01}Ge_{1-x}Sb_x$ alloy thin films

3.1.1 Introduction

The group IV based semiconducting materials such as Germanium (Germanium is discovered by Clemens A. Winkler at Freiberg, Germany in 1886), doped with small concentration of magnetic ions have extensively been studied for its application in spintronics **[1-9]**. In solid state electronics and semiconductor physics, Germanium (Ge) may be used as an intrinsic semiconductor which forms the starting point for the fabrication. Ge is an indirect band gap semiconductor having a high refractive index, possessing small effective mass and high mobility as compared with Silicon (Si). Germanium has more free electrons and a higher conductivity at a given temperature. The addition of a small percentage of other atoms in the crystal lattice of Ge, produces dramatic changes in their electrical properties as well as other properties and doping produces n- type and p-type semiconductors. The band theory suggests that p-type and n-type semiconductors show extra energy levels in addition of impurities. The changes in the properties due to doping resulted in various studies on Ge using different doping **[1-3]**.

The ferromagnetic ordering observed in transition metal doped Ge thin films **[4-5]** and bulk systems **[6-7]** has shown Curie temperatures (T_c) well below RT. However, RT ferromagnetism is reported in GeMn, $Ge_{1-x}Mn_x$ compound thin films **[8-9]** & also in some ternary compound semiconductors like $(Cd_{0.8}Mn_{0.2})GeP_2$ **[10]** and $(Zn_{0.94}Mn_{0.06})GeP_2$ **[11]**. Somayajulu *et. al.* also observed hyperfine magnetic interactions at RT in Fe doped Ge based bulk system with doping of V-VI group donor impurities **[12]**. Yusuke Shuto *et. al.'s* **[13]** study of Fe concentration dependence in $Ge_{1-x}Fe_x$ ($x = 0.02$ to 0.24) thin films reported magnetism for $x \leq 0.13$. The Curie temperature is well below RT at ~170 K. R. Goswami *et. al.'s* **[14]** study on Fe doping

in Ge results in the formation of ferromagnetic nanoparticles Fe_3Ge_2. A study by S.H. Song *et. al.* **[15]** in $Ge_{1-x}Fe_x$ thin films for x = 0.04 to 0.40, prepared by thermal co-evaporation technique showed saturation magnetization of 2.40 emu/cm^3 for x = 0.04. Recently published articles by Nam Hee Kim *et al.* **[16]** and Carl M. Liebig *et. al.* **[17]** reported the effects of Ag doping on the crystallization properties of Sb rich GeSb thin films and Phase-transitions in GeSb induced by customized ultrafast optical pulses respectively. Study by T.B. Massalski *et. al.* **[18]** showed possible compounds in the binary Ge-Fe system as $FeGe_2$, FeGe, Fe_6Ge_5, and Fe_3Ge. All these compounds are non-magnetic.

In one of the earlier study by Narendra Patel *et. al.* **[19]** reported the bulk $Fe_{0.008}Ge_{1-x}Sb_x$ system (at x = 0.00) in the absence of Sb, no magnetic interaction is observed. But when Sb is incorporated in this system hyperfine magnetic field is observed at Fe site. A Microscopic technique Mossbauer spectroscopy is used to see the magnetic interaction in the bulk system at RT. The authors observed magnetic interaction (*i.e.* hyperfine magnetic field) at Fe site for Sb ($0.01 < x < 0.05$) concentration, which evinces the magnetic interaction is Sb concentration dependent on the bulk system **[19]**.

In this chapter the various studies of donor impurity (Sb) doped in Ge host lattice with extremely small concentration of Fe (0.01) thin films are discussed. No reports are found in which the Fe doping in Ge thin films is investigated for such a low concentration.

3.1.2 Experimental details

$Fe_{0.01}Ge_{1-x}Sb_x$ (x = 0.01, 0.05 and 0.10) bulk alloys are prepared by melting desired quantities of constituting elements having > 99.99% purity under argon atmosphere in an arc furnace. The details of argon arc furnace are discussed in chapter

2. The alloys are re-melted many times to ensure homogeneity. The ingots of bulk alloys are grounded to a fine powder and then thin films are grown on Silicon (Si) substrate by thermal evaporation technique. The details of thermal evaporation technique are also discussed in chapter 2. The powdered alloys are loaded in a crucible and evaporated with resistive heating at $>10^{-5}$ Torr. After deposition, these thin film samples are annealed at a temperature of 400 ^{o}C for 1 hour at 5×10^{-5} Torr to release stress and to achieve better adhesion of film with substrate. The thickness of the films is ~ 500 nm measured using Fizeau fringes for all concentration of Sb. The various characterizations for the $Fe_{0.01}Ge_{1-x}Sb_x$ (x = 0.01, 0.05 and 0.10) thin films are conducted at UGC DAE CSR Indore, India.

3.1.3 Structural studies

Structural characterization of the $Fe_{0.01}Ge_{1-x}Sb_x$ thin films is done using Grazing Angle X-ray diffraction (GAXRD) by Bruker D8 advance X-ray diffractometer technique with CuK_α radiation (wavelength 1.54 Å).

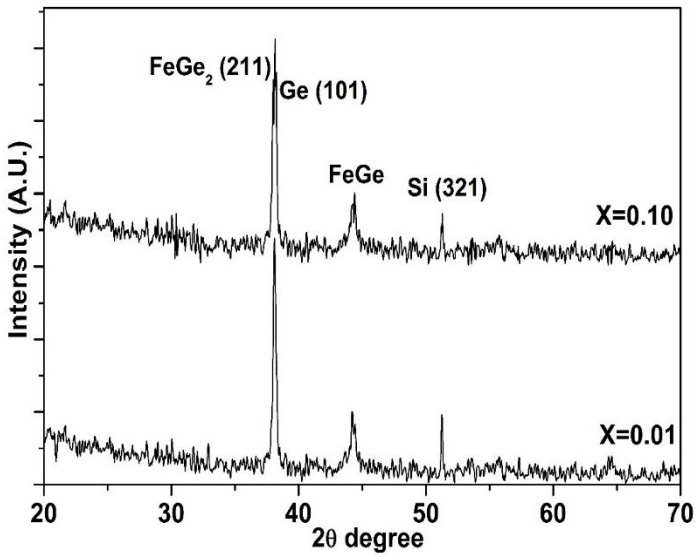

Figure 3.1: *XRD spectra of dilute Fe doped $Ge_{1-x}Sb_x$ thin films for x = 0.01 and 0.10*

The X-rays are detected using a fast counting detector based on Silicon strip technology (Bruker LynxEye detector). X-ray diffraction patterns of the as deposited

$Fe_{0.01}Ge_{1-x}Sb_x$ (x = 0.01 and 0.10) thin films are shown in **figure 3.1**. In this diffraction pattern the reflection at $2\theta \approx 51.3^o$ is due to the (321) reflection of Silicon substrate (ASTM-JCPDS card No.72-1426), while two merged sharp diffraction peaks located at $2\theta \approx 38.2^o$ is identified as reflections of Ge (101) (ASTM-JCPDS card No. 65-0334) and $FeGe_2$ (211) (ASTM-JCPDS card no. 89-1982) **[12]**. The other diffraction peaks at $2\theta \approx 44.3^o$ are due to FeGe reflection (ASTM-JCPDS card No. 20-0516) **[12]**. There is a slight shift in the position of the peaks and variation in the intensity showing the dopants are going into the substitutional sites in parent element Ge.

Crystallite size is calculated by using Debye Scherrer Formula $D = 0.89\lambda/\beta\cos\theta$, in which D is crystallite size, λ is wavelength of X-rays, θ is Bragg angle and β is Full width at half maxima (FWHM). The calculated crystallite size from observed highest intense peak and minimum 2θ value at $2\theta \approx 38.2^o$ is found to be ~ 29 nm and 32 nm for x = 0.01 and 0.10 respectively.

3.1.4 Electrical studies

To measure the effect of temperature on the resistivity of film, the whole resistivity set up unit is kept in a cryostat and the resistance is measured by Keithley 617 programmable electrometer connected to DC Power supply **[20]**. These electrical resistance measurements are performed by the conventional Two-Probe method in the temperature range 200-400 K for different Sb (x = 0.01, 0.05, 0.10) concentration.

The **figure 3.2** shows a plot of resistivity as a function of temperature of $Fe_{0.01}Ge_{1-x}Sb_x$ films for the temperature range of 220- 400 K. This curve depicts that, with the increase in temperature of the $Fe_{0.01}Ge_{1-x}Sb_x$ thin film resistivity decreases which indicates the semiconducting nature of the thin films having a negative temperature coefficient of resistance **[21]**. **Figure 3.3** shows the Arrhenius curve, plotted in between $\ln \rho$ versus $(10^3/T)$.

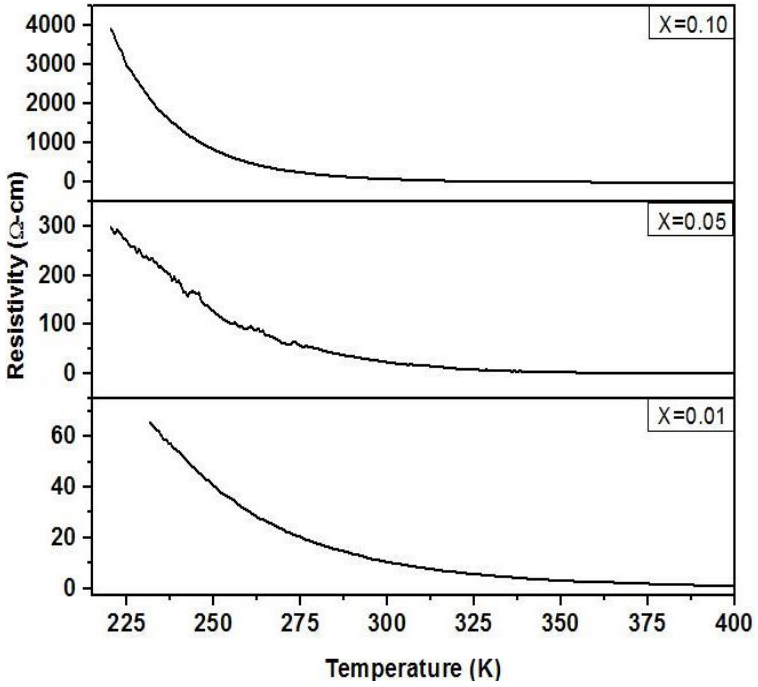

Figure 3.2: *Resistivity versus temperature spectra of $Fe_{0.01}Ge_{1-x}Sb_x$ thin films for x = 0.01, 0.05 and 0.10 respectively*

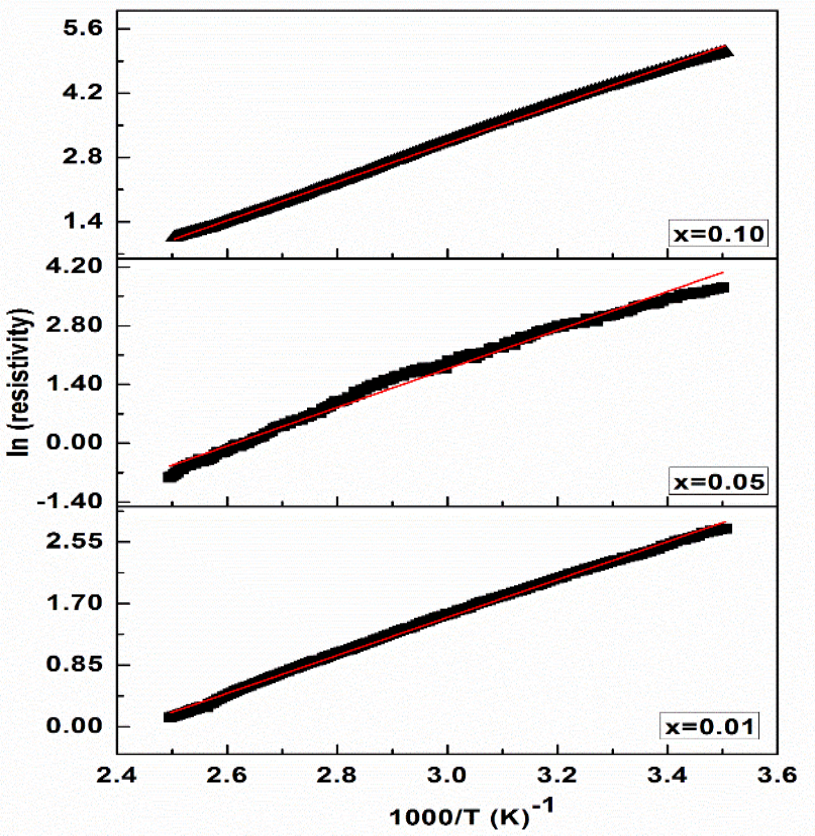

Figure 3.3: *Log (Resistivity) vs (10^3/T) spectra of $Fe_{0.01}Ge_{1-x}Sb_x$ thin films for x = 0.01, 0.05 and 0.10 grown on Silicon substrate*

This curve shows that with the increase in Sb concentration, the electrical resistivity increased for a particular temperature due to decrease in carrier concentration. This change in electrical resistivity indicates that the doped atoms are contributing to the carrier concentration and mobility.

These resistivity data have been used to obtain the activation energy using Arrhenius equation *i.e.*

$$R(t) = R_0 \exp(E_a/K_bT)$$

Where R(t) is resistivity at temperature T, E_a is the activation energy and K_b is the Boltzmann constant. The variation of Activation Energy versus concentration of Sb (x) for $Fe_{0.01}Ge_{1-x}Sb_x$ thin film is plotted in **figure 3.4**.

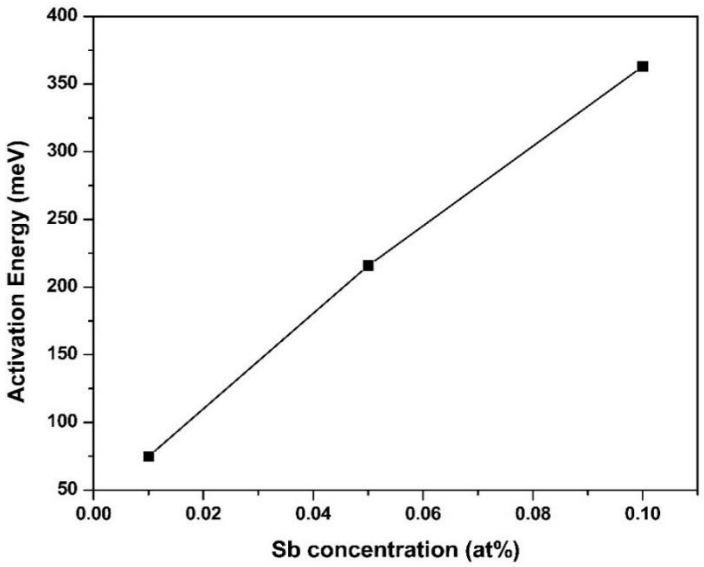

***Figure 3.4**: Activation energy vs Concentration of Sb (x) plot of $Fe_{0.01}Ge_{1-x}Sb_x$ thin films*

It is observed from **figure 3.4** that activation energy linearly increases with the increase in Sb concentration. This suggests that due to inclusion of Sb in the system the width of energy band gap increases, which increases the resistivity and hence decreasing the conductivity of Fe doped $Ge_{1-x}Sb_x$ thin films. These results also support our argument of contribution of charge carriers in the Ge matrix.

In order to explain the low temperature transport mechanism in Fe doped $Ge_{1-x}Sb_x$ thin films, variable range hopping model has been used. The variable range hopping model is discussed with its detail in chapter 1. For this the plotted log of normalized resistivity as a function of $(1/T)^{1/4}$ with Variable Range Hopping mechanism (VRH) as suggested by Ambegokar *et. al.* **[22]** shown in **figure 3.5**. The VRH mechanism is governed by

$$\rho(T) = \rho_0 \exp(T_0/T)^{1/4}$$

where ρ_0 and T_0 denote material parameters, and $T_0 = [1.5 / K_B\alpha^3 N(E)]$, where N(E) is the density of states at the Fermi level and α denotes the rate of fall-off of the envelops of the electron wave function **[23]**. The plot for lnρ versus $(1/T)^{1/4}$ is shown in **figure 3.5**.

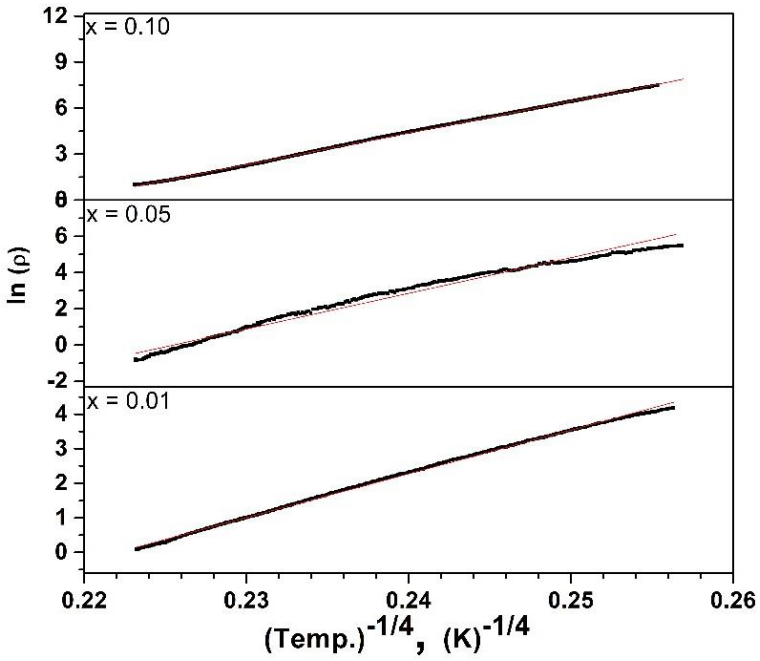

Figure 3.5: *Temperature dependence of ρ(T) measured in $Fe_{0.01}Ge_{1-x}Sb_x$ thin films, by the relation based on the three dimensional Mott's variable range hopping conduction (3D-VRH), using equation $\rho(T) = \rho_0 exp(T_0/T)^{1/4}$. The solid red lines are the linear fits of the data*

The plotted curve in between lnρ versus $(1/T)^{1/4}$ linearly fitted (red lines are fitted curve in **figure 3.5**) and compared with the $\rho(T) = \rho_0 \exp(T_0/T)^{1/4}$ equation. From the slope of

the curve, the value of T_0 has been obtained for Fe doped $Ge_{1-x}Sb_x$ thin films. It is observed that the value of T_0 increases with increase in Sb concentration for x = 0.01, 0 05, 0.10 respectively. This suggests that the density of states at the Fermi level decreases with increase in Sb concentration. The density of states also decreases with increase in resistivity for the Fe doped $Ge_{1-x}Sb_x$ system. The above results corroborate the hopping of charge carriers between randomly distributed localized electronic states in the Fe doped $Ge_{1-x}Sb_x$ thin films.

3.1.5 AFM studies

Root Mean Squared (rms) surface roughness and particle size are determined by AFM from Digital Instruments (Nanoscope III) with Si_3N_4 tip under ambient conditions in contact mode. The surface morphology is studied by AFM for the Fe doped $Ge_{1-x}Sb_x$ thin films. **Figure 3.6** show 2-d images of $Fe_{0.01}Ge_{1-x}Sb_x$ thin film for x = 0.01, 0.05 and 0.10 respectively. From the AFM images it is observed that the average particle size for $Fe_{0.01}Sb_{1-x}Se_x$ thin films increases from 35 to 60 nm when the Sb concentration increases for x = 0.01 to 0.10.

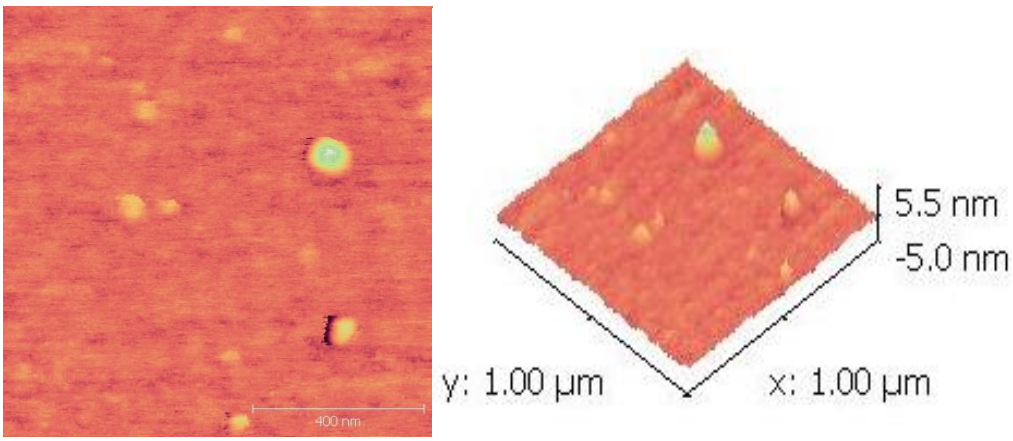

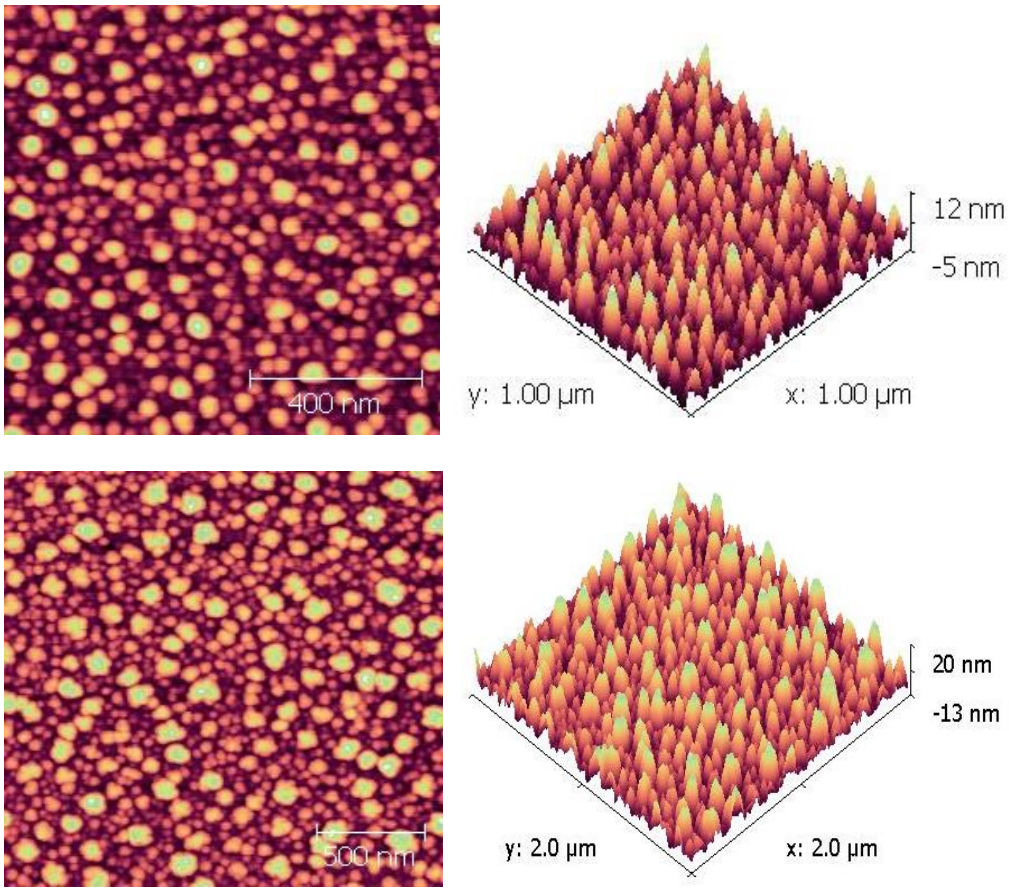

Figure 3.6: *Surface morphological image (AFM image) of $Fe_{0.01}Ge_{1-x}Sb_x$, left side 2-D and right side 3-D, for x = 0.01, 0.05 and 0.10 respectively*

The variation of particle size rms and roughness variation with their standard deviation for different Sb concentration is shown in **table 3.1**.

Sample composition	Atomic Force Microscope	
$Fe_{0.01}Ge_{1-x}Sb_x$	Average Particle size (nm) with standard deviation	Average rms roughness over $1\times1\mu m^2$ (nm)
x = 0.01	35±4	1.7
x = 0.05	45±4	3.7
x = 0.10	60±4	5.6

Table 3.1: *Surface structural parameters calculated from Atomic Force Microscopy for different Sb concentration, x = 0.01, 0.05 and 0.10 respectively*

From the **table 3.1** it is seen that the surface smoothness with rms roughness measured over $1\times1\mu m^2$ is significantly high and it is in the range of 1.7 to 5.6 nm for different concentration of Sb. It is to be noted that the average particle size determined using

AFM is higher than the crystallite size determined using XRD. It suggests that the particles observed in the AFM images are not single crystals but are made-up of few crystallites. It can be seen from the AFM images that the density of the crystals is quite high. Such particles are uniformly distributed over the thin film surface and seem to be predominantly due to crystallites of Ge matrix.

3.1.6 Magnetic Force Microcopy studies

The MFM study is carried out to investigate the magnetic domain structure of $Fe_{0.01}Ge_{1-x}Sb_x$ films. **Figure 3.7** shows topography AFM images (left side) and corresponding MFM images (right side) of thin films. The MFM images are taken performed with atomic force microscope operating in tapping/lift mode, which combines interaction and constant height mode in order to separate short range topography and magnetic signals **[24-25]**. Because the Van der Waals forces only become significant for tip-sample distances < 10 nm whereas magnetic measurements can be alleviated by using enough lift heights > 17 nm.

To observe the effect of Sb concentration variations in magnetic interactions for the $Fe_{0.01}Ge_{1-x}Sb_x$ thin films, MFM images are collected for various Sb concentrations *i. e.*, x = 0.01, 0.05 and 0.10 respectively. These AFM and MFM images differ in contrast respectively, which appears to decorate the topology. Magnetic contrast is visible in all the samples, consistent with uniform in-plane magnetization of the films.

However, the weak contrast in the MFM image indicates the absence of Fe or Fe related magnetic compound or clusters with Ge and Sb magnetic clusters which should give a clear contrast and strong magnetic response **[26-27]**.

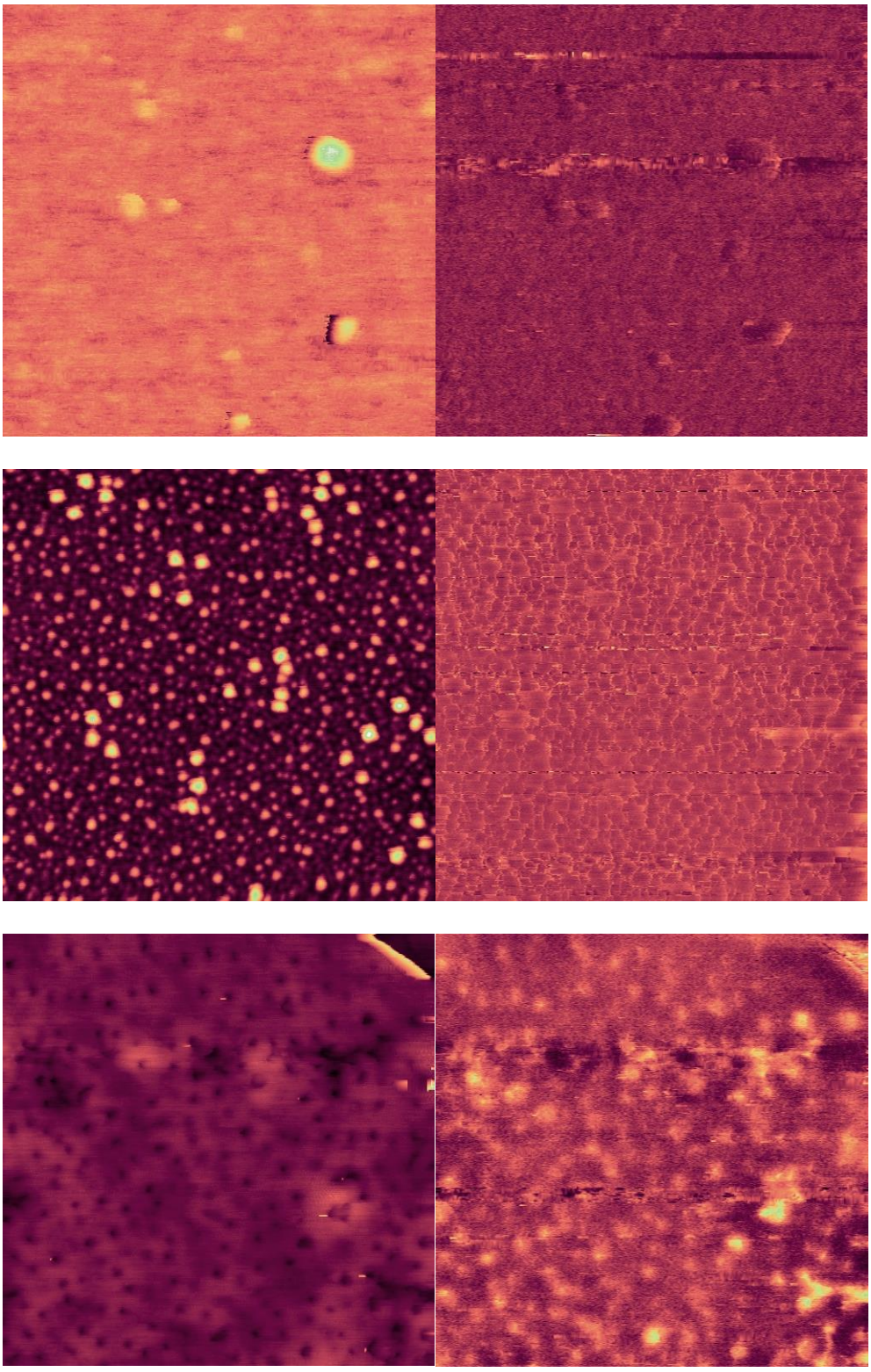

Figure 3.7: *Topography image (AFM image) left side and corresponding MFM image right side with the same area of 1×1 mm^2 for $Fe_{0.01}Ge_{1-x}Sb_x$,x = 0.01, x = 0.05 and x = 0.10 respectively*

When we compare MFM images corresponding to different Sb concentrations such difference is considerable. Such small difference in magnetic signal contrast indicates the existence of magnetic interactions, but these signals are comparatively quite weak. The average magnetic domain sizes are calculated using the MFM images. The domain size increases from 43 to 68 nm with an increase in Sb concentration for x = 0.01 to 0.10 as shown in **figure 3.8**.

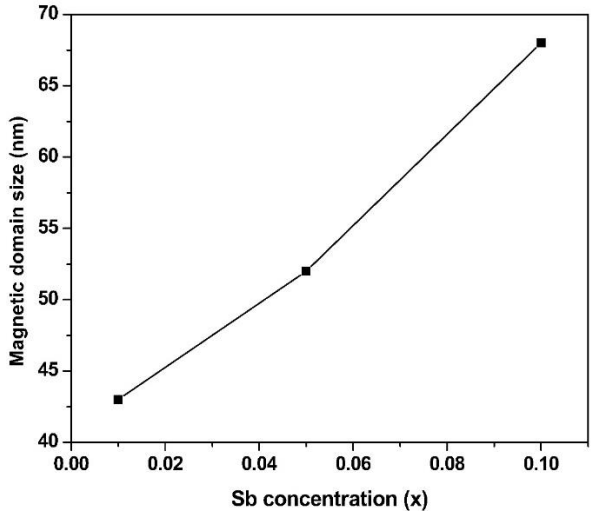

Figure 3.8: *Magnetic domain size vs with Sb concentration variation (x) of $Fe_{0.01}Sb_{1-x}Se_x$ thin films*

There is a linear behavior of the magnetic domains with increase in concentration of Sb (x). In the $Fe_{0.01}Ge_{1-x}Sb_x$ thin film system. Fe acts as an acceptor in Ge, while Sb acts as a donor in Ge. With Sb addition, Sb brings charge carriers into the system, thus compensating for the holes brought by Fe in Ge. The magnetic moment on Fe (d-state) appears to be polarized due to sp-d exchange interaction through the itinerant carriers introduced by Sb (sp state) doping in Ge matrix. The mechanism behind the magnetic behavior for the Fe-Ge-Sb system seems to be same as the one observed by the Somayajulu *et. al.* in the $Fe_{0.008}Sb_{1-x}Se_x$ bulk system **[28]**.

3.2 Effects of SHI beam on $Fe_{0.01}Ge_{1-x}Sb_x$ thin films

3.2.1 Introduction

The defect plays a crucial role in stabilizing the ferromagnetic state in dilute magnetic semiconductors **[29-33]**. Certain types of defects or disorder favor ferromagnetism and others compete with this phenomenon. The Energetic ion beam irradiation is an important tool for introducing defect states in solid materials. The Swift Heavy Ion (SHI) beam loses energy mainly through inelastic collisions with atomic electrons. Along the trajectory, a trial of defects such as point defects, defect clusters, structural phase transition etc., may be formed. The type of formation depends on the type of ion and its energy as well as physical property of the materials. The radiation damage is developed in the neighborhood of the path of the ion beam. These ions beam modifies the material through electronic excitation followed by slowing down of swift heavy ions in the material.

The irradiation using SHI is an important technique for controlled modifications of structural, optical, surface and magnetic properties of the semiconductors **[34-35]**. There are several reports where the effects of ion beam irradiation on transition metal doped different semiconductors as ZnO **[36-40]**, TiO_2 **[41]** and Ge **[42-44]** based semiconductors are found. Look *et. al.* **[36]** and Hayes *et. al.* **[37]** reported the effects of light and heavy ion irradiation in ZnO films. In the Germanium based semiconductors, P. Marie *et. al.* **[42-44]** reported that the defects are created due to SHI irradiation in n- type **[42]** and p type **[43]** Germanium. The ion beam irradiation induced modification of different physical properties and the role of defects in the Germanium based semiconductor is reported **[42-44]**. But No studies observed, which explains the ion irradiation induced effects on Germanium based dilute magnetic semiconductor thin films.

Dilute magnetic semiconducting material offers the advantage of the spin degree of freedom and compatibility with existing semiconductor technologies **[45-47]** which is extremely important for spintronics, potential technological applications such as tunable ferromagnetic devices using carrier-induced ferromagnetism **[48-49]** and high efficient spin injectors into a Semiconductor **[50]**. In the group IV based semiconducting materials **[51-53]** long range ferromagnetic ordering is observed at different temperatures. In the one of earlier study by Narendra Patel *et. al.* **[54]** observed the hyperfine magnetic interactions at RT in Fe doped Ge based bulk DMS system containing V and VI group donor impurities.

These studies were the motivation to see the effect of these bulk alloys in the form of thin films and also to investigate the effects of swift heavy ion irradiation on the physical properties of dilute magnetic semiconducting thin films. An attempt has been made to analyze the change in structural, electrical and surface properties of $Fe_{0.01}Ge_{1-x}Sb_x$ (x = 0.01 and 0.10) alloy thin films due to irradiation with a fluence of 1×10^{12} ions/cm^2 with O^{7+} beam.

3.2.2 Experimental details

Firstly, the bulk alloys of Fe doped $Ge_{1-x}Sb_x$ system are prepared by melting desired quantities of constitute elements having 99.99 % purity under argon atmosphere in an arc furnace. The alloys are re-melted many times to ensure homogeneity. The ingot of bulk alloys is grinded to fine powder and then the thin films are prepared on Silicon substrate by thermal evaporation technique. The experimental details of thermal evaporation technique and Argon arc furnace is discussed in chapter 2. The powdered alloys are loaded in a crucible and evaporated with resistive heating at >10^{-5} Torr. After deposition, the sample are annealed at the high temperature 600 ^oC for 1 hour to release stress and to achieve better adhesion of film and substrate. The thickness of the films is

~ 500 nm measured using fizaue fringes. The fizaue fringe method is discussed in chapter 2.

These thin films are irradiated with 100 MeV O^{7+} ions using a 15 UD Tandem Accelerator, at Inter University Accelerator Centre (IUAC) New Delhi **[55]** (details of palletron accelerator are discussed in chapter 1) with the fluence of 1×10^{12} ions/cm^2. The ion beam is focused to a spot of 1 mm diameter and scanned over a 1.2×1.2 cm^2. The radiation beam is defocused to cover the whole sample. To observe the structural, electrical and surface effects due to the Swift heavy ion irradiation on the $Fe_{0.01}Ge_{1-x}Sb_x$ thin film, Grazing Angle X-ray diffraction (GAXRD), Two Probe Resistivity measurements and Atomic Force Microscope (AFM) are performed respectively.

3.2.3 Structural studies

Structural characterization is done using the GAXRD technique with CuK_α radiation (wavelength 1.54 Å). X-ray diffraction pattern of the as deposited and irradiated with O^{+7} for $Fe_{0.01}Ge_{1-x}Sb_x$ (x = 0.01 and x = 0.10) thin films shown in **figure 3.9(a)** and **3.9(b)** respectively. In the XRD pattern of as deposited film **figure 3.9(a)**, the reflections are due to Silicon substrate, $FeGe_2$ and FeGe compound phases

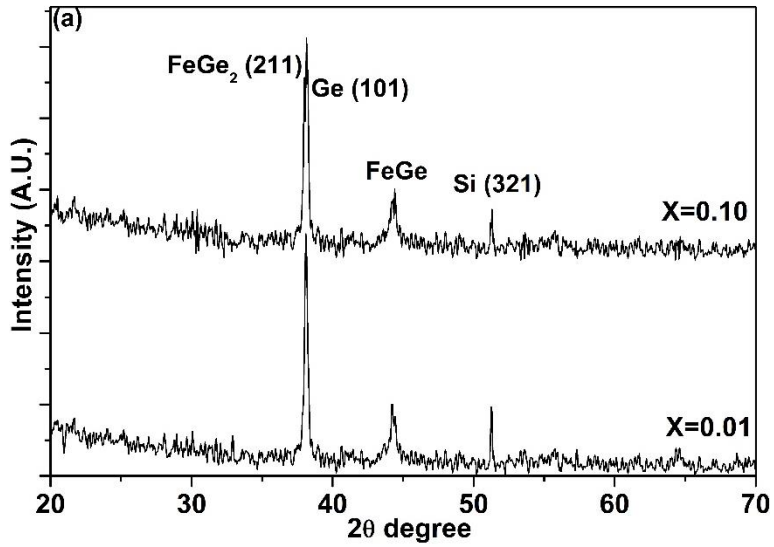

Figure 3.9(a): *X-ray diffraction pattern of as deposited $Fe_{0.01}Ge_{1-x}Sb_x$ thin film*

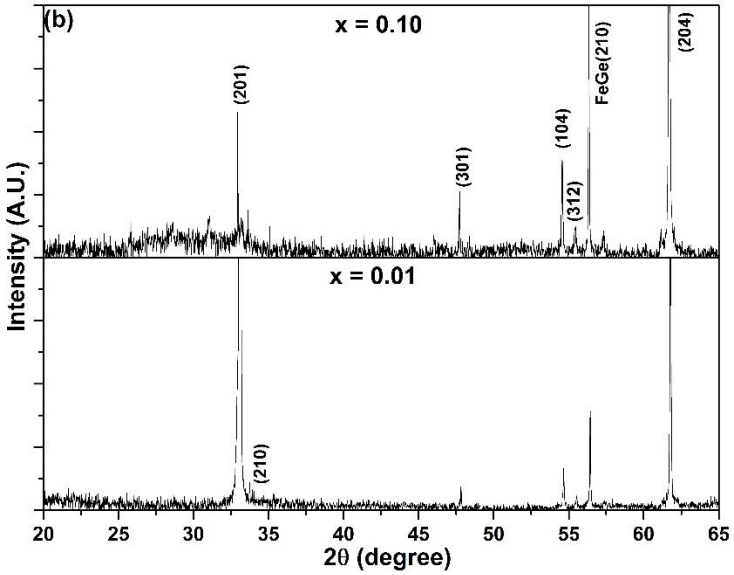

Figure 3.9(b): *X-ray diffraction pattern of irradiated with O^{+7} having 100 MeV energy $Fe_{0.01}Ge_{1-x}Sb_x$ thin film*

The XRD pattern of irradiated $Fe_{0.01}Ge_{1-x}Sb_x$ film **figure 3.9(b)** reveals the reflection is only due to Ge phase. The crystallite size for irradiated film is calculated using Debye Scherrer formula, for the values of x = 0.01 and 0.10. Crystallite size for both the concentrations of Sb is ~29 nm.

3.2.4 Electrical studies

Resistivity measurements are performed by the conventional Two-Probe technique. Two probe method is discussed with details in chapter 2. **Figure 3.10** shows resistivity versus temperature plot for un-irradiated and irradiated thin films in the temperature range of 270-350 K for x = 0.01 (left side) and x = 0.10 (right side) of Sb concentration respectively. The resistivity of all the films decreases with increase in temperature clearly indicating the semiconducting property of the materials **[56]**. It is observed from **figure 3.10** that resistivity lies in this range even after irradiation where the electrical resistivity is ~ 15 Ω-cm for x = 0.01. But in case of x = 0.10 after irradiation resistivity increases dramatically.

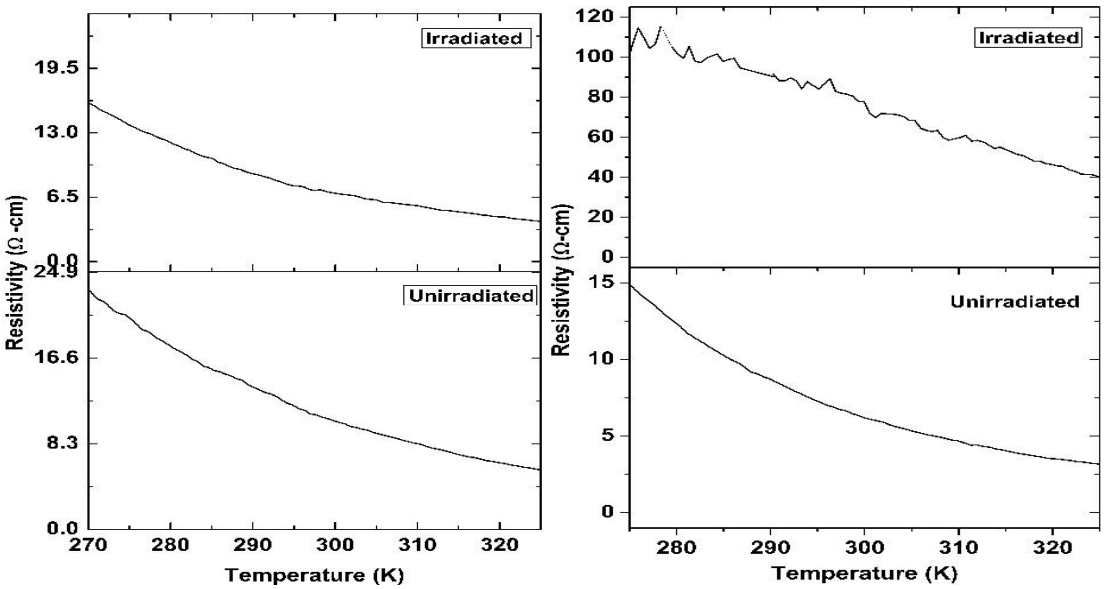

Figure 3.10: *Temperature dependence Resistivity study of $Fe_{0.01}Ge_{1-x}Sb_x$, un-irradiated and irradiated with O^{7+} ions, Energy 100 MeV, with fluence 1×10^{12} ions/cm^2 for left side x = 0.01 and right side x = 0.10 respectively*

The increase in resistivity after irradiation seems to be due to compound phase formation in Fe-Ge-Sb alloy like $FeSb_2$, which is more likely as the concentration of Sb is quite high. The exposure to irradiation for a long time appears to anneal the sample at an extremely high temperature, which results in the formation of the compound phase, thereby increase in the resistivity of the alloy film at x = 0.10. The formation of compound phase decreases the charge carriers in the thin films resulting in a dramatic increase in resistivity to ~115 Ω-cm for a temperature of 275 K.

This resistivity data has been used to obtain the activation energy using Arrhenius equation *i.e.*

$$R(t) = R_0 \exp(E_a/K_bT)$$

Where R(t) is resistivity at temperature T, E_a is the activation energy and K_b is the Boltzmann constant. The comparative results of Activation Energy before and after irradiation for $Fe_{0.01}Ge_{1-x}Sb_x$, x = 0.01 and 0.10 is listed in **table 3.2**.

It is observed from **table 3.2** that after irradiation of $Fe_{0.01}Ge_{1-x}Sb_x$ thin films with O^{+7} ions at 100 MeV energy with fluence of 1×10^{12} ions per cm^2, the activation energy decreases for x = 0.01 and its increases for x = 0.10 respectively.

Sample Composition $Fe_{0.01}Ge_{1-x}Sb_x$	Activation Energy (meV)	
	Un-irradiated	irradiated
x = 0.01	225	207
x = 0.10	362	408

Table 3.2: *Resistivity measurement results of un-irradiated and irradiated O^{+7}, 100 MeV, 1×10^{12} ions/cm^2 thin films grown at Si substrate*

3.2.5 AFM studies

The surface topographies of the un-irradiated and irradiated $Fe_{0.01}Ge_{1-x}Sb_x$ thin films are analyzed by Atomic Force Microscopy. The working principle and details of AFM is discussed in chapter 2. The AFM images of the un-irradiated and the irradiated thin films for $Fe_{0.01}Ge_{1-x}Sb_x$, x = 0.01 and x = 0.10 are shown in **figure 3.11** respectively.

The reduction of surface roughness and increase in particle size are evident from the surface topography. The average particle size for x = 0.01 is found to be ~ 40-43 nm for un-irradiated and ~52-57 nm for irradiated thin film and for x = 0.10, the average particle size is found to be ~60-80 nm for un-irradiated and 90-100 nm for irradiated thin films respectively. The measured root mean squared surface roughness for $Fe_{0.01}Ge_{0.99}Sb_{0.01}$ un-irradiated thin film is 1.72 nm and after irradiation it is found to be 0.31 nm over the 1×1 μm^2 area and for $Fe_{0.01}Ge_{0.90}Sb_{0.10}$ for un-irradiated thin film surface roughness is 5.58 nm and after irradiation it is found to be 4.64 nm over the 1×1 μm^2 area respectively. The particle size and root mean squared surface roughness is given in **table 3.3**.

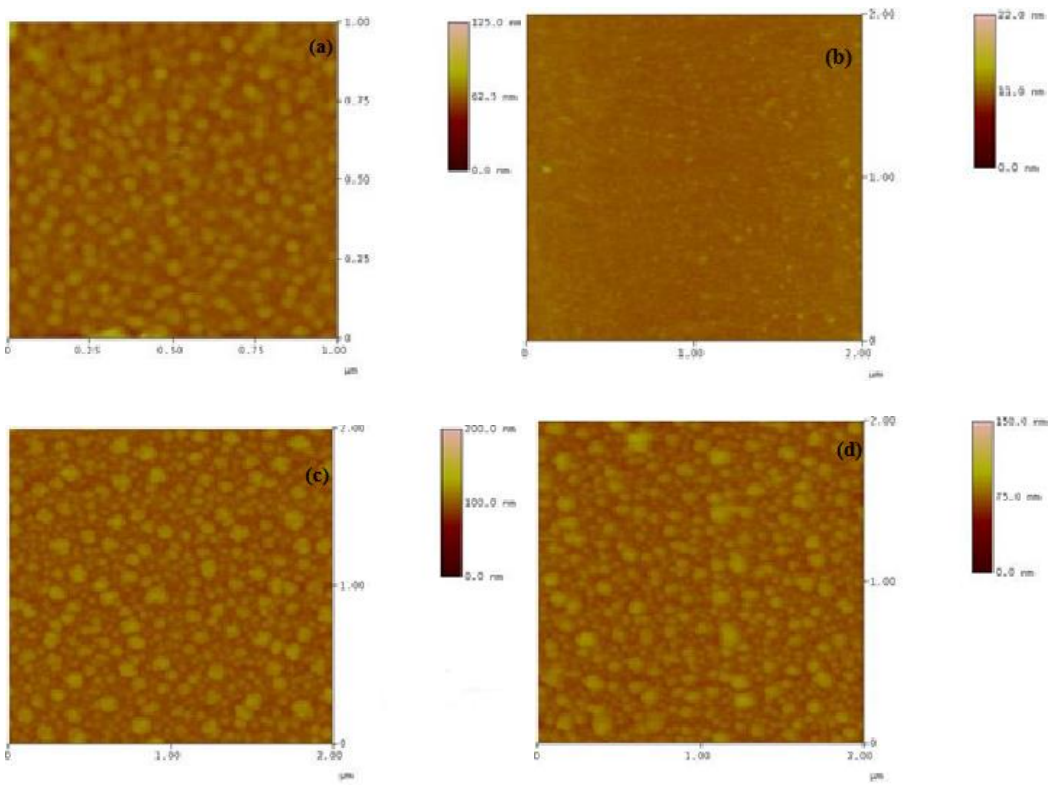

Figure 3.11: *AFM topography images of $Fe_{0.01}Ge_{1-x}Sb_x$ thin films (a) un-irradiated and (b) irradiated (O^{7+}, 100 MeV with fluence 1×10^{12} ions/cm^2) for x = 0.01 & topography image (c) and (d) shows the morphology image of un-irradiated and irradiated for x = 0.10 respectively*

Sample Composition $Fe_{0.01}Ge_{1-x}Sb_x$	Roughness (Over the 1x1 μm^2 areas measured)		Particle Size (nm)	
	unirradiated	Irradiated	unirradiated	irradiated
x = 0.01	1.72	0.31	40-43	52-57
x = 0.10	5.58	4.64	60-80	90-100

Table 3.3: *Surface morphological parameters of un-irradiated and irradiated thin films, irradiated with O^{+7} ions, energy 100 MeV, and fluence 1×10^{12} ions/cm^2*

From the surface morphology images, it is found to be that the particle size determined using AFM are higher than the crystallite size which is determined using XRD. This indicates that the particles observed in the AFM images are not single crystals but are made-up of few crystallites. Surprisingly irradiation with high energy beam instead of reducing the particle size increases the size. It could be due to annealing process taking place by prolonged exposure of the sample to the beam.

References

[1] S. Tari, R. Sporken, T. Aoki, David J. Smith, V. Metlushko, K. AbuEl-Rub and S. Sivananthan *J. Vac. Sci. Technol. B* **20** 4 (2002).

[2] R. Goswami, G. Kioseoglou, A. T. Hanbicki, O. M. J. van 't Erve, B. T. Jonker, and G. Spanos *Appl. Phys. Lett.* **86** 032509 (2005).

[3] O. Kazakova, R. Morgunov, J. Kulkarni, J. Holmes, and L. Ottaviano *Phys. Rev. B* **77** 235317 (2008).

[4] Wang Yong, Zou Jin, Zhao Zuoming, Han Xinhai, Zhou Xiaoyu and Wang Kang L. *J. Appl. Phys.* **103** 066104 (2008).

[5] Y. Fukuma, H. Asada, J. Miyashita, N. Nishimura and T. Koyanagi *J. Appl. Phys.* **93** 7667 (2003).

[6] S. M. Sze and J. C. Irvin *Solid State Electron.* **11** 599 (1968).

[7] Sungyoul Choi, Cheol Hong Soon, Sunglae Cho, Yunki Kim, John B. Ketterson, Chin Un Jung, and Y. C. Kim *J. Appl. Phys*. **93** 7670 (2003).

[8] Sung Kyu Kim, Yong Chan Cho, Se-Young Jeong, Chae- Ryong Cho, Sang Eon Park, J. H. Lee, Kim Jong Pil, Y. C. Kim and H. W.Choi *Appl. Phys. Lett.* **90** 192505 (2007).

[9] Hong Liang Li, Yihong Wu, Zaibing Guo, Ping Luo, Shijie Wang *J. Appl. Phys.* **100** 103908 (2006).

[10] Gennadiy A. Medvedkin, Takayuki Ishibashi, Takao Nishi, Koji Hayata, Yoichi Hasegawa and Katsuaki Sato *Jpn. J. Appl. Phys. Part 2* **39** L949 (2000).

[11] Sunglae Cho, Sungyoul Choi, Gi-Beom Cha and Cheol Hong Soon *Phys. Rev. Lett.* **88** 257203 (2002).

[12] D. R. S. Somayajulu, Narendra Patel, Mukesh Chawda, Mitesh Sarkar & K C. Sebastian *Indian Journal of Pure and Appl. Phys.* **44** 129 (2006).

[13] Yusuke Shuto, Masaaki Tanaka, Satoshi Sugahara *Appl. Phys Lett.* **90** 132512 (2007).

[14] R. Goswami, G. Kioseoglou, A. T. Hanbicki, O. M. J. van't Erve, B. T. Jonker, and G. Spanos *Appl. Phys. Lett.* **86** 032509 (2005).

[15] S.H. Song, S.H. Lim *J Magn and Magn Mater* **304** 64 (2006).

[16] Nam Hee Kim, Hyung Keun Kim, Kyu Min Lee, Hyun Chul Sohn, Jae Sung Roh, Doo Jin Choi *Thin solid films* **519** 5323 (2011).

[17] Carl M. Liebig, E. Audouard, J. Solis, Razvan Stoian, *Optical Materials* **33** 1210 (2011).

[18] T.B. Massalski (Ed.) Binary Alloy Phase Diagrams, vol. 2, second ed. *American Society for Metals Cleveland* 1706 (1990).

[19] Narendra Patel, Mitesh Sarkar, Mukesh Chawda and D R S. Somayajulu *Solid State Physics* India Vol. **54** 995 (2009).

[20] N Badera, Bhavana Godbole, S. B. Shrivastava, P. N. Vishwakarma, L. S. Sharadchandra, Deepti Jain, V. G. Sathe, V. Ganesan *Sol. Energy Mater. Sol Cells* **92** 1646 (2008).

[21] Y. X. Chen, Shi Shen Yan, Y. Fang, Y.F. Tian, S. Q. Xiao, G. L. Liu, Y. H. Liu, L.M. Mei *Appl. Phys. Lett.* **90** 052508 (2007).

[22] Vinay Ambegaokar, B. I. Halperin, J. S. Langer *Phys. Rev. B* **8** 4 (1971).

[23] Shubra Singh, M. S. Ramchandra Rao *Phys. Rev. B* **80** 045210 (2009).

[24] S. A. Koch, R.H.te Velde, G Palasantzas, J.Th. M. De Hosson *Appl. Phys. Lett.* **84** 556 (2004).

[25] S. Porthum, L. Abelmann and C. *J.* Lodder *Magn. Mater* **182** 238 (1998).

[26] F. Singh, D. K. Awasthi, O. Angelov, P. Berthet, J. C. Pivin, *Nucl. Instrum. Meth B* **245** 214-218 (2006).

[27] C. B. Fitzgerald, M. Venkatesan, L. S. Dorneles, R. Gunning, P. Stamenov, and J. M. D. Coey, P. A. Stampe, R. J. Kennedy, E. C. Moreira, U. S. Sias *Phy. Rev. B* **74** 115307 (2006).

[28] D. R. S. Somayajulu, Mukesh Chawda, Narendra Patel, M Sarkar, K.C. Sebastian, K. Venugopalan, A. Gupta *Appl. Phys. Lett.* **87** 242508 (2005).

[29] X L. Li, X H. Xu, Z Y Quan, J F Guo, H S Wu and G A Gehring *J. Appl. Phys.* **105** 103914 (2009).

[30] B Straumal B, A A Mazilkin, S G Protasova, A A Myatiev, P B Straumal, G Schütz, Aken P A van, E Goering and B Baretzky *Phys. Rev. B* **79** 205206 (2009).

[31] S Dutta, S Chattopadhyay, A Sarkar, M Chakrabarti, D Sanyal and D Jana *Prog. Mater. Sc.* **54** 89 (2009).

[32] J B Yi *et. al. Phys. Rev. Lett.* **104** 137201 (2010).

[33] S Chattopadhyay, S K Neogi, A Sarkar, M D Mukadam, S M Yusuf, A Banerjee and S J. Bandyopadhyay *J Magn. Magn. Mat.* **323** 363 (2011).

[34] S Kumar, R Kumar and D P Singh *Appl. Sur. Sc.* **255** 8014 (2009).

[35] B Angadi, Y S. Jung, W K Choi, R Kumar, K Jeong, S W. Shin, J H. Lee, J H. Song, M W Khan and J P Srivastava *Appl. Phys. Lett.* **88** 142502 (2006).

[36] D C Look, D C Reynolds, J W Hemsky, R L Jones and J R Sizelove *Appl. Phys. Lett.* **75** 811 (1999).

[37] M Hayes, F D Auret, Rensburg P J J van, J M Nel, W Wesch and E Wendler *Nucl. Instru. Meth.Phys. Res. B* **257** 311 (2007).

[38] H. Zang et al. *Nucl. Instru. Meth. Phys. Res. B* **266** 2863 (2008).

[39] D C Agarwal, A Kumar, S A Khan, D Kabiraj, F Singh, A Tripathi, J C Pivin, R S Chauhan and D K Avasthi *Nucl. Instru. Meth. Phys. Res. B* **244** 136 (2006).

[40] P M R Kumar, K P Vijayakumar and C S Kartha *J. Mater. Sci.* **42** 2598 (2007).

[41] Hardeep Thakur, Ravi Kumar, P. Thakur, N. B. Brookes, K. K. Sharma, Abhinav Pratap Singh, Yogesh Kumar, S. Gautam and K. H. Chae *J. Appl. Phys.* **110** 083718 (2011).

[42] P. Marie, M. Levalois, and P. Bogdanski *J. Appl. Phys.* **74 (2)** (1993).

[43] P. Marie, M. Levalois, and E. Paumier *J. Appl. Phys.* **79** 7555 (1996).

[44] P. Marie and M. Levalois *J Appl. Phys.* **75** 1852 (1994).

[45] Y. B. Xu, E. Ahmad, J. S. Claydon et al. *J. Magn. Magn. Mater.* **304** 69 (2006).

[46] G. A. Prinz *Science* **282** 1660 (1998).

[47] S. A. Wolf *Science* **294** 1488 (2001).

[48] S. Koshihara, A. Oiwa, M. Hirasawa, S. Katsumoto, Y. Iye, C. Urano, H.Takagi, and H. Munekata *Phys. Rev. Lett.* **78** 4617 (1997).

[49] H. Ohno, D. Chiba, F. Matsukura, T. Omiya, E. Abe, T. Dietl, Y. Ohno, and K. Ohtani *Nature (London)* **408** 944 (2000).

[50] Fiederling, M. Keim, G. Reuscher, W. Ossau, G. Schmidt, A. Waag, and L. W. Molenkamp *Nature (London)* **402** 787 (2002).

[51] S Choi, S Hong, S Cho, Y Kim, J Ketterson, C Jung, K Rhie, B Kim and Y Kim *J. Appl. Phys.* **93** 7670 (2003).

[52] Y. D Park, A. Hanbicki, S Erwin, C Hellberg, J Sullivan, J Mattson, T Ambrose, A Wilson, G Spanos, B Jonker *Science* **295** 651 (2002).

[53] Y Fukuma, M Arifuku, H Asada and T Koyanagi *J. Appl. Phys.* **91** 7502 (2002).

[54] Narendra Patel, Mukesh Chawda, Mitesh Sarkar K. C Sebastian, D. R. S. Somayajulu and Ajay Gupta *Hyp. Int.* **160** 247 (2005).

[55] http://www.iuac.res.in/accel/pell/index.html

[56] Y. X. Chen, Shi-shen Yan, Y. Fang, Y. F. Tian, S.Q.Xiao, G.L.Liu, Y. H. Liu, L.M. Mei *Appl. Phys. Lett.* **90** 052508 (2007).